J Appl Electrochem (2011) 41:1373–1379
DOI 10.1007/s10800-011-0339-3

SHORT COMMUNICATION

Electrochemical recycling of cobalt from spent cathodes of lithium–ion batteries: its application as coating on SOFC interconnects

Eric M. Garcia · Hosane A. Tarôco · Tulio Matencio · Rosana Z. Domingues · Jacqueline A. F. dos Santos · Marcos B. J. G. de Freitas

Received: 20 June 2011 / Accepted: 15 July 2011 / Published online: 29 July 2011

Abstract In this work the metallic cobalt was electrodeposited on 430 steel in order to obtain a low electrical resistance film made to Co_3O_4. Pure cobalt was obtained by acidic dissolution of lithium cobalt oxide ($LiCoO_2$) present in exhausted Li-ion battery cathode. The electrodeposition was performed with a 96% efficiency at a potential of 1.50 V versus Ag/AgCl. The electrodeposited cobalt showed the face-centered cubic (23%) and hexagonal centered (77%) phases. After oxidation at 850 °C for 1000 h in air, the cobalt layer was transformed into the Co_3O_4 phase. On the other hand, a sample without cobalt showed the usual Cr_2O_3 and $FeCr_2O_4$ phases. After 1000 h at 850 °C, in air the area specific resistance of the sample with the cobalt oxide layer was 0.038 Ω cm^{-2}, while it was 1.30 Ω cm^{-2} for the bare sample.

Keywords Li-ion batteries · Cobalt · Recycling · Solid oxide fuel cell · Electrodeposition · Interconnect

1 Introduction

1.1 Electrical interconnects of solid oxide fuel cells (SOFCs)

Solid oxide fuel cells (SOFCs) are solid-state devices that produce electricity by electrochemically combining fuel and air across an ionically conducting electrolyte [1–3]. In order to obtain high voltage and power density, a number of individual cells consisting of a porous anode, a dense thin-film electrolyte, and a porous cathode are electrically connected by interconnects to form a "stack". These interconnects are in contact with both electrodes (cathode and anode) and must meet a number of requirements [2–4]:

- Low area specific resistance (ASR). An acceptable value, after 40,000 working hours, is 0.10 Ω cm^{-2}.
- Chemical stability in both atmospheres (reducing and oxidant) at high temperatures (between 600 and 1000 °C).
- Impermeability to O_2 and H_2.
- Linear thermal expansion coefficient, LTEC, compatible with the other components of the cell (value close to 12.5 × 10^{-6} K^{-1}).

Metallic interconnects have attracted a great attention due to their high electronic and thermal conductivity and a low cost and good manufacturability compared to traditional ceramic interconnects [6, 7]. In recent years, many works have been focused on ferritic stainless steel due to its low cost and adequate linear thermal expansion coefficient (11–12 × 10^{-6} K^{-1}) [5–7]. However, under the cathode working conditions (typically 1123 K in air) CrO_3 and $CrO_2(OH)_2$ evaporate from the Cr_2O_3 oxide film formed on the surface of this material [7, 8] causing severe cell degradation. To improve the surface electrical properties and reduces the amount of chromium in the oxide film a coating of the stainless steel with semiconductor oxides has been proposed [8, 9]. Cobalt oxide Co_3O_4 is a promising candidate because of its interesting conductivity of 6.70 S cm^{-1} and an adequate LTEC [7, 8, 10]. A good strategy to obtain the Co_3O_4 layer over stainless steel is cobalt electrodeposition with subsequent oxidation in air at high temperatures

E. M. Garcia (✉) · H. A. Tarôco · T. Matencio · R. Z. Domingues · J. A. F. dos Santos
Chemistry Department, Federal University of Minas Gerais, Av. Antônio Carlos, 6627, Pampulha, MG 13565-905, Brazil
e-mail: ericmgmg@hotmail.com

M. B. J. G. de Freitas
Chemistry Department, Federal University of Espírito Santo, Av. Fernando Ferrari, 514, Goiabeiras, ES 29075-910, Brazil

(SOFC cathode conditions) [9, 10]. The cobalt electrodeposition can be a low cost [11–18] technique. Moreover, very pure cobalt can be obtained by acidic dissolution of lithium cobalt oxide ($LiCoO_2$) present in spent Li-ion battery cathode [12–15]. This recycling of $LiCoO_2$ is important both economically and environmentally [12]. Thus in this work, cobalt metal was electrodeposited over 430 stainless steel with a subsequent oxidation at 850 °C in air to form the Co_3O_4 layer. The scanning electron microscope (SEM) and X-ray diffraction (XDR) measurements were used to characterized this oxide formation. We focused our experimental observations on the stability of this layer and on the resulting improvement of the ferritic steel ASR.

2 Experimental

2.1 Preparation of cobalt electrodeposition solutions

Li-ion batteries were manually dismantled and physically separated into their different parts: anode, cathode, steel, separators, and current collectors. The cathodes were dried at 400 °C for 24 h and washed with distilled water at 40 °C for 1 h under agitation to eliminate organic solvents and to facilitate the detachment of the active material from the respective current collectors. The active material was filtered and washed with distilled water at 40 °C to remove possible lithium salts such as $LiPF_6$ and $LiCl_4$ and dried in air for 24 h. A mass of 250.10 g of positive electrodes was dissolved in an aqueous solution containing 470.00 mL of H_2SO_4 3.00 mol L^{-1} and 30.00 mL H_2O_2 30% v/v. The system was maintained under constant magnetic agitation at 80 °C for 2 h. The cathode dissolution efficiency increases with the increase of the acid concentration and temperature. The addition of H_2O_2 is also necessary to increase the efficiency of the cathode dissolution. The H_2O_2 reduces the (+III) cobalt, insoluble in water, to the (+II)oxidation state, soluble in aqueous solution (Eq. 1) [12].

$$2LiCoO_{2(s)} + 2H_2O_{2(aq)} + 3H_2SO_{4(aq)} \rightarrow 2CoSO_{4(aq)} + 3/2O_{2(g)} + Li_2SO_{4(aq)} + 5H_2O_{(l)} \quad (1)$$

The pH of the electrodeposition baths was controlled to a value of 3.0 and the cobalt concentration was 3.10 mol L^{-1}. This high concentration was chosen to increase the electrodeposition efficiency.

2.2 Electrochemical measurements

Electrochemical measurements were made using a AUTOLAB PGSTAT power supply. The working electrode was made of commercial ferritic stainless steel 430. Its composition is shown in Table 1. The steel samples were prepared as rectangular foils with a geometric area of 1.00 cm^2. The auxiliary electrode, with an area of 3.75 cm^2,

Table 1 Composition of stainless steel 430 (wt%)

Mn	Si	Cr	Ni	Co	W	Al	Fe	C	S
0.48	0.008	17.0	0.06	0.007	0.015	0.012	82.3	0.0482	0.002

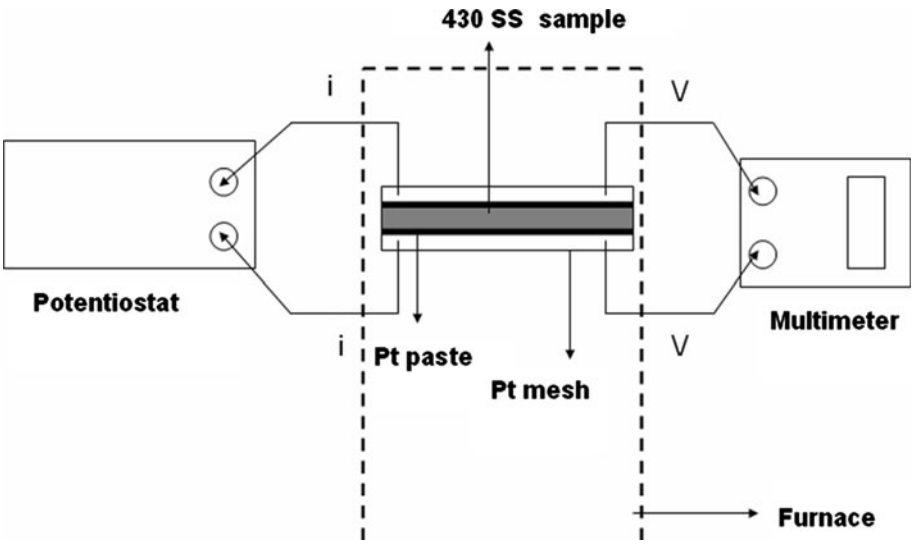

Fig. 1 Diagram of the area specific resistance measurement cell

was made of platinum. A saturated Ag/AgCl reference electrode was used. The working electrodes were sanded with 600-grit sandpaper before each measurement and washed with distilled water. In the potentiodynamic measurements, the initial and final potential polarizations were −0.50 and −1.00 V, respectively. The potential scan rate was 20 mV s^{-1}. Potentiostatic measurements were made applying cobalt reduction potentials of: −0.80, −0.90, −0.90, −1.20, −1.50, and −2.00 V. The charge density (Q) applied at each potential reduction was 30.0 C cm^{-2}. The charge efficiency was calculated using the Faraday law. All the electrochemical measurements were performed without solution agitation, at 25 °C.

2.3 Interconnect characterization

The oxidation behavior of a commercial stainless steel 430 coated with an electrodeposited cobalt layer ion was investigated at 850 °C in air and compared to the oxidation behavior of the non-coated alloy. The ASR was measured using a DC four-probe method on the experimental sandwich structure shown in Fig. 1. The sample was initially heated up at a rate of 20 °C min^{-1} to 850 °C and held at this temperature for 1000 h. During the long-term test, a constant current density of 200 mA cm^{-2} was applied with the AUTOLAB PGSTAT power supply and the voltage was recorded by a digital Multimeter 8808A FLUKE. The ASR was calculated according to Ohm's law. All the above-mentioned tests were made in a box furnace and static air. The scanning electron microscope JEOL JXA model 8900 RL, equipped with an energy dispersive X-ray (EDX) detector, was used for the surface morphology observations and surface chemical analysis. The cobalt coating was examined by XRD before and after 1000 h of oxidation (Fig. 1). The equipment used was a 200 B Rotaflex-Rigaku with a copper Kα radiation, Ni filter, and scan speed of 0.02° min^{-1}.

3 Results and discussion

3.1 Cobalt electrodeposition

The chemical composition of deposition bath plays an important role during the electrodeposition [12, 13]. At pH 3.00, the predominant Co(II) chemical species is the $[Co(H_2O)_6]^{2+}$ complex. The cobalt electrodeposition process follows Eq. 2:

$$\left[Co(H_2O)_6\right]^{2+} + 2e^- \rightarrow Co^0 + 6H_2O \quad (2)$$

Figure 2 presents a typical potentiodynamic curves for 430 stainless steel in a solution with cobalt concentration of 3.10 mol L^{-1} and a solution with sodium sulfate concentration equals 3.10 mol L^{-1} both in pH 3.00. During the first cathodic scan, the current density starts to increase at −0.98 V. For solution without cobalt, the reduction current (Eq. 3) only becomes significant at potentials lowers than −1.40 V.

$$H^+ + H_2O + 2e^- \rightarrow OH^- + H_2 \quad (3)$$

The reverse scanning shows an increase in the ionic cobalt electrodeposition current because electrodeposition happens on the cobalt previously electrodeposited (Fig. 2). Moreover it was noted that the cobalt dissolution (Eq. 4) occurs at potentials higher than −0.34 V.

$$Co^0 + 6H_2O \rightarrow \left[Co(H_2O)_6\right]^{2+} + 2e^- \quad (4)$$

Figure 3 shows the charge efficiency of the cobalt electrodeposition at different potentials. The maximum efficiency of 96.0% is at a potential equals to −1.50 V. At lower potentials, the charge efficiency decreases. This is probably due to water and hydrogen proton reduction (Eq. 3). This hypothesis is confirmed by the voltammetry diagram shown in Fig. 2.

3.2 Samples characterizations

3.2.1 X-ray diffraction analysis

Cobalt exists in two distinct crystallographic phases. One phase has a hexagonal closed packed (hcp) structure and a symmetry space group *P*63/*mmc* with an ICSD number 52935. The other phase has a face centered cubic (fcc) structure with a symmetry space group *Fm*-3*m* and an

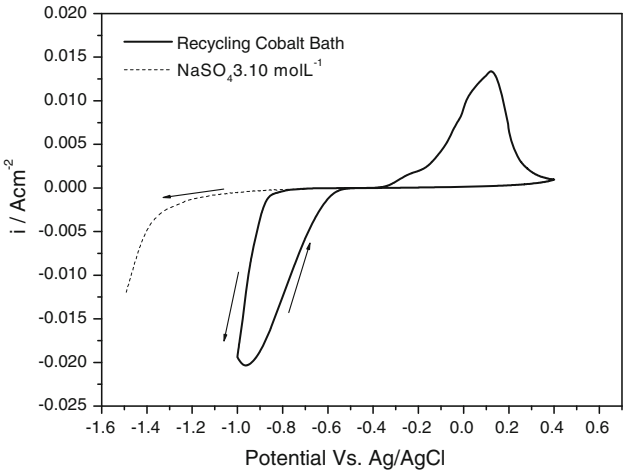

Fig. 2 Cyclic voltammetry of a 430 ferritic steel in a solution of sodium sulphate (3.0 mol L^{-1}) and cobalt sulphate obtained by recycling Li-ion batterie cathodes. The potential scan rate was 20 mV s^{-1}

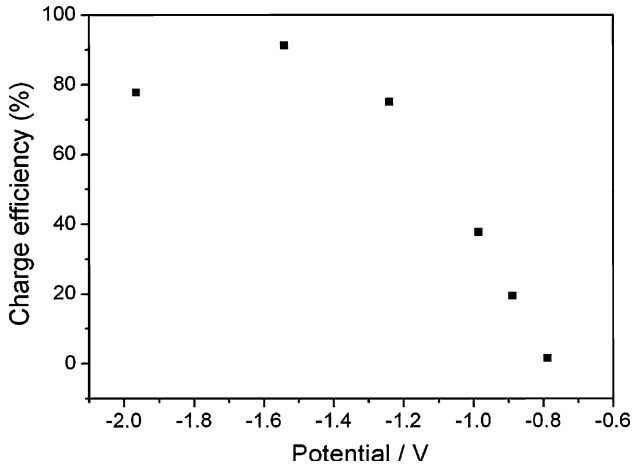

Fig. 3 Charge efficiency of the cobalt electrodeposition process at different potential values

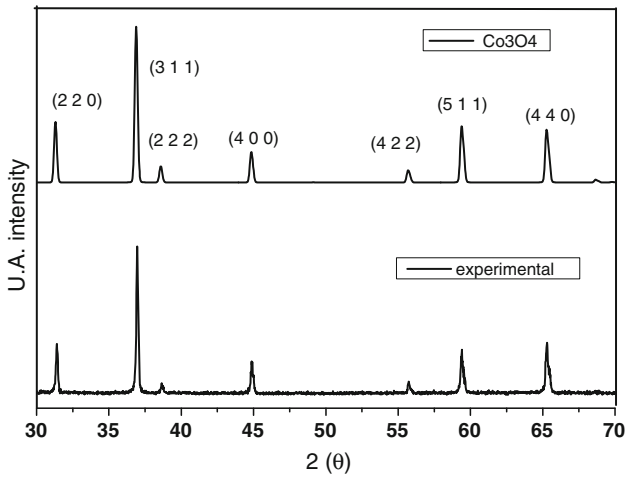

Fig. 5 X-ray diffractogram of the cobalt electrodeposited on 430 ferritic steel and oxidized in air at 850 °C for 1000 h. Theoretical diffraction patterns of the Co_3O_4 spinel

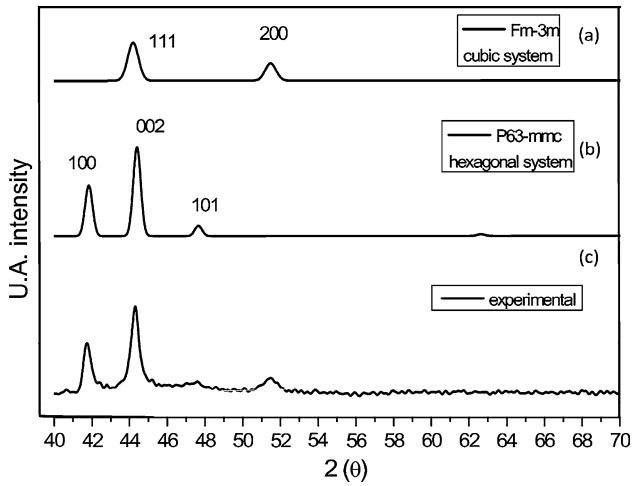

Fig. 4 Theoretical diffraction patterns of cubic cobalt (*a*) and hexagonal cobalt (*b*) X-ray diffractogram of the electrodeposited cobalt (*c*) with charge density 30.0 C cm^{-2} and potential −1.5 V

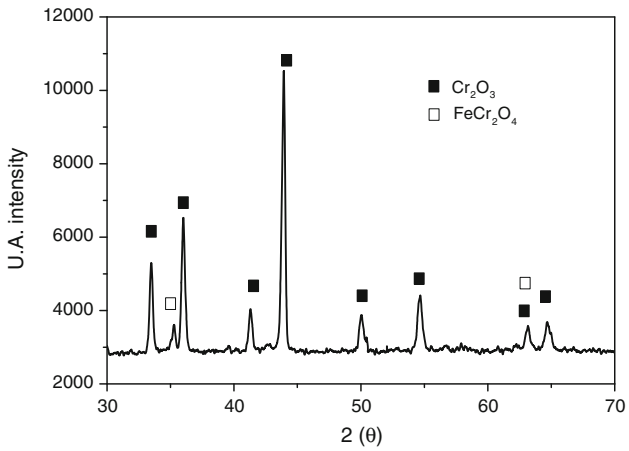

Fig. 6 X-ray diffractogram of 430 bare steel surface oxidized in air at 850 °C for 1000 h

ICSD number 53805. The transformation energy (ε_{trans}) between the high-temperature face-centered cubic (fcc) phase and the stable hexagonal closed packed (hcp) phase is determined by the stacking fault energy. It is very low ($\gamma_{st} = 25 \times 10^{-3}$ J m^{-2}) [19]. During the cobalt electrodeposition the formation of the cobalt fcc is promoted by the co-deposition of atomic hydrogen. During and after the electrodeposition, the fast diffusion of the hydrogen causes the formation of the more stable hcp phase. Figure 4a shows the X-ray diffractogram of electrodeposited cobalt. Figure 4b and c gives the theoretical diffraction patterns of the hexagonal and cubic cobalt, respectively. From the Full Prof software (copyright© 2010) it was possible to calculate the percentage of each phase. The cubic phase amounts to 23% and the hexagonal phase to 77%. Figure 5 shows the X-ray diffractogram of the electrodeposited cobalt after oxidation at 850 °C for 1000 h. The presence of cobalt oxide Co_3O_4 (ICSD 27497) on the 430 steel was confirmed by the simulation software performed using the Full Prof software (copyright© 2010).

For comparison, Fig. 6 shows the X-ray diffraction pattern of bare 430 ferritic steel after oxidation at 850 °C for 1000 h. The diagram shows that the main phase formed on this sample surface is Cr_2O_3 with an ICSD number 167284. A small amount of $FeCr_2O_4$ ICSD number 43269 was also observed. This result clearly demonstrates that a Co_3O_4 coating reduces the growth rate of the Cr_2O_3 layer.

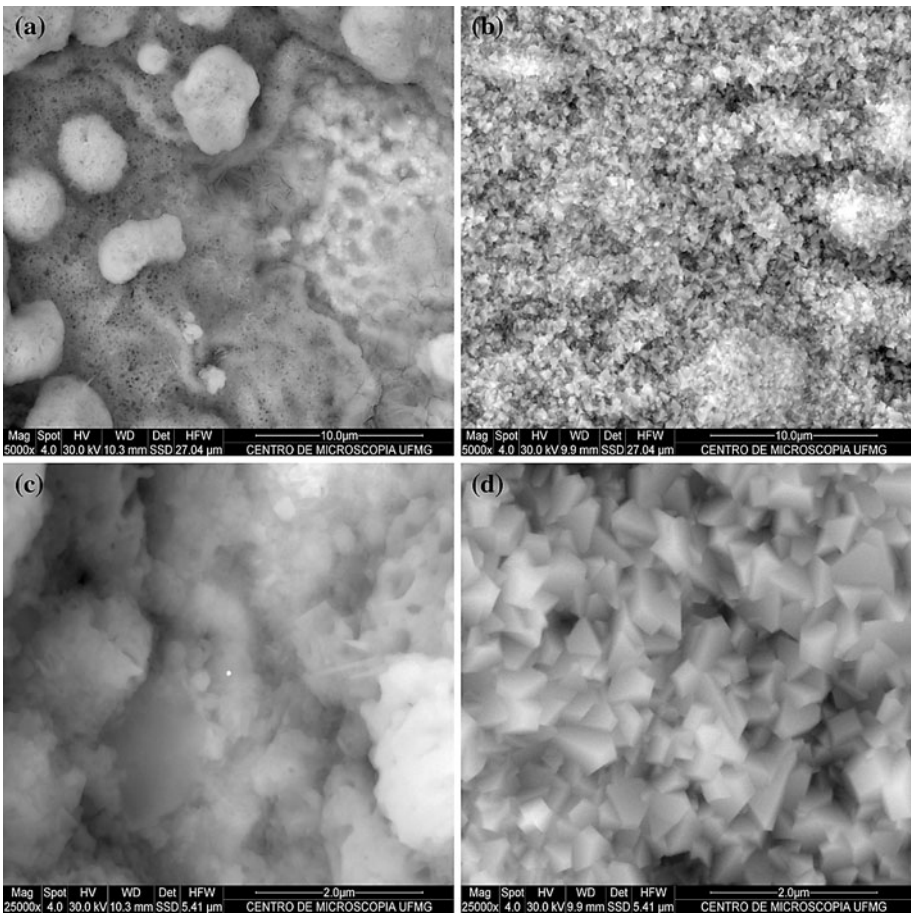

Fig. 7 Scanning electron microscopy images (SEM) of 430 ferritic steel surfaces cobalt oxide not covered **a** magnification of ×5,000 and **c** ×25,000 and cobalt oxide covered **b** magnification of ×5,000 and **d** ×25,000, after oxidation in air at 850 °C for 1000 h

3.2.2 *Scanning electron microscopy (SEM) and energy dispersive X-ray (EDX) analysis*

The morphology is very important because it is related with the electrical losses caused by the electrical resistance. The electrical resistance is represented by $R = (L\rho)/A$, where L is the thickness, A is the contact area of sample, and ρ the resistivity. Then the greater the thickness of the sample, the greater the total electrical resistance [1]. Moreover, the smaller the contact area, the greater the electrical resistance. The stainless steels have acceptable corrosion tolerance (slow kinetics for oxide growth). Consequently the effects of decreased electrical contacts are more important than the thickness increase for samples submitted to high temperatures in oxidant atmosphere [1, 2, 5].

The porosity increasing is one of the causes of contact losses. Figure 7 shows the scan electron micrographs (SEM) of 430 steel samples with and without cobalt coating after oxidation in air atmosphere, for 1000 h, at 850 °C. The steel samples without cobalt coating, Fig. 7a and c, shows the presence of porosity and oxide spallation. The surface steel degradation occurs due formation of volatile Cr(VI) species (Eq. 5) under an oxidizing environment [1, 4].

$$Cr_2O_{3(s)} + 3/2O_{2(g)} \rightarrow 2CrO_{3(g)} \quad (5)$$

In an effort to avoid this problem, it was applied conductive cobalt spinel (Co_3O_4) coatings which were deposited on the surface of 430 stainless steel by electrodeposition and subsequent air oxidation. The SEM images to steel sample with Co_3O_4 coating, as seen in Fig. 7b and d, shows the presence of numerous cubic structures, consistent with spinel formation. Also, compared with Fig. 7a and c it can be seen that the porosity and oxide spallation has been significantly reduced. The sample covered with cobalt shows a more regular morphology than uncoated one. The Co_3O_4 coatings serve as a barrier to decrease the Cr_2O_3 in the surface of the samples as shows in the EDX measurements (Fig. 8b). In the sample without cobalt (Fig. 8a) the presence of chromium is due to formation of Cr_2O_3 and $FeCr_2O_4$. The Mn is probably related to the metallic substrate.

It seems thus that electroplating followed by oxidation is a promising method for the fabrication of spinel protective coatings for SOFC interconnects made of ferritic stainless steels.

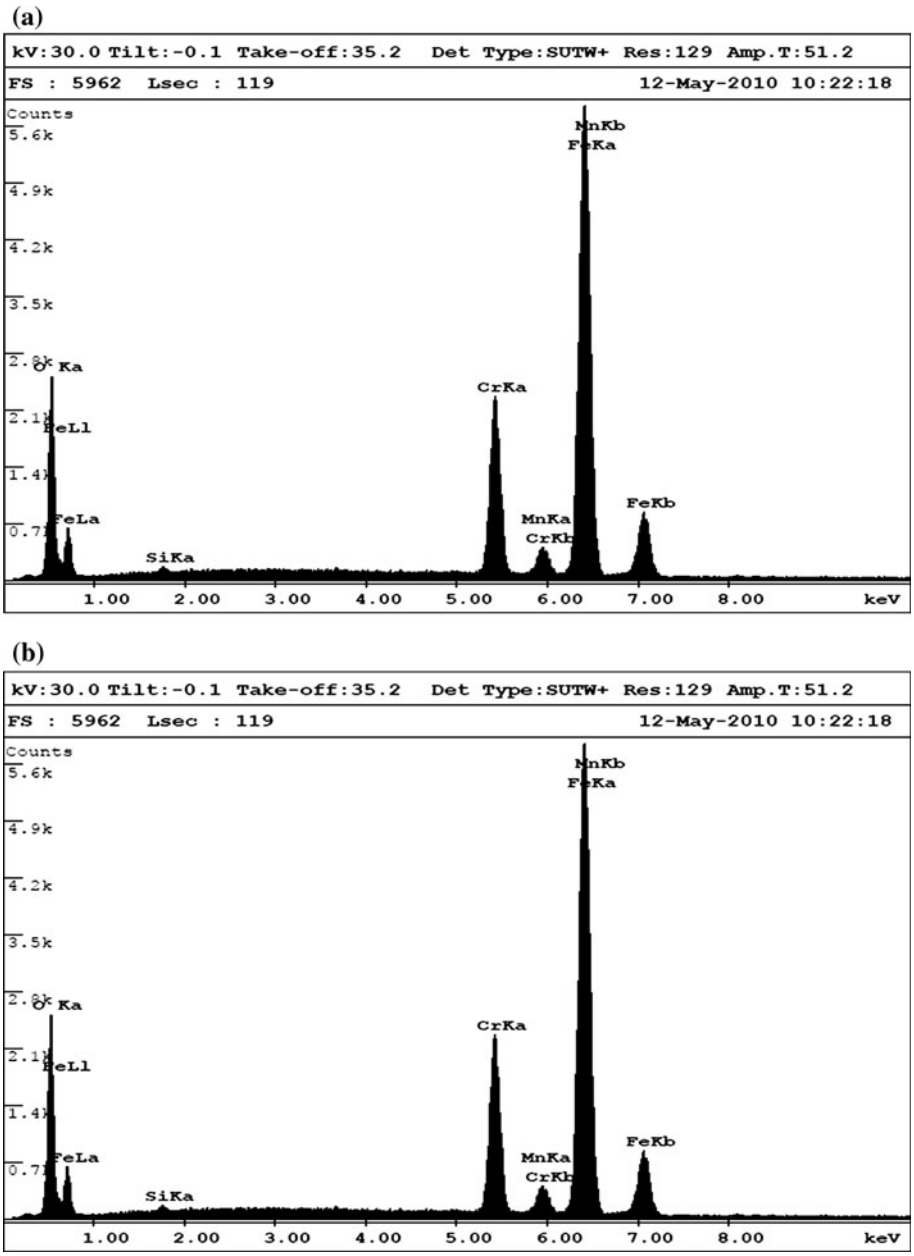

Fig. 8 X-ray Dispersive Energy (XDE) of 430 ferritic steel covered without cobalt oxide (**a**) and with cobalt oxide (**b**) oxidized in air at 850 °C for 1000 h

3.2.3 Area specific resistance

Figure 9 shows the ASRs of 430 steel samples with and without cobalt coating after oxidation in air for 1000 h at 850 °C. The sample with cobalt oxide coating has a lower resistance compared to that of the bare sample. This is obviously related to the different natures of the oxide films formed on the samples. The conductivity of Cr_2O_3 is 1.1×10^{-2} S cm^{-1} and the Co_3O_4 is 6.7 S cm^{-1}. After 400 h, the sample without cobalt showed a great increase in its ASR value. This may be due to fragmentation of the oxide film that results into a loss of electric contact. After 1000 h the ASR value of the sample without cobalt was 1.30 Ω cm^{-2}. For the sample with a cobalt oxide film this value was only 0.038 Ω cm^{-2}.

4 Conclusion

The cobalt electrodeposition was successfully performed with a 96% efficiency at a potential of 1.50 V. The electrodeposited cobalt showed the fcc (23%) and hcp (77%) phases. After oxidation at 850 °C for 1000 h the steel surface presented the Co_3O_4 phase. On the other hand, a sample without deposited cobalt showed mainly the Cr_2O_3 phase. The cobalt electrodeposition improves the electrical

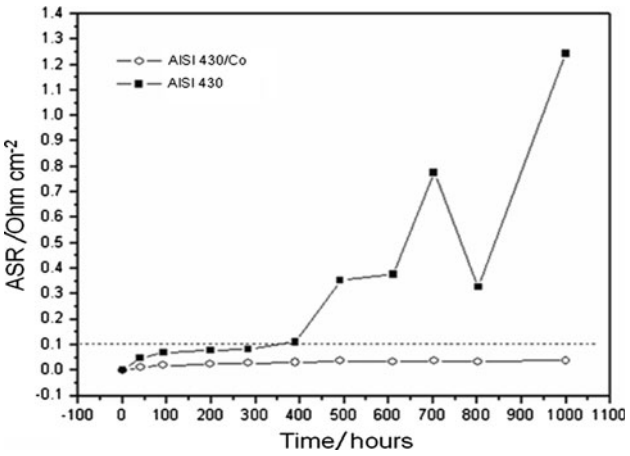

Fig. 9 Area specific resistance of 430 stainless ferritic steel with and without cobalt oxide coating. Oxidation at 850 °C for 1000 h

and morphological characteristics of the 430 ferritic steel. In the analyzed intervals of time the 430 steel with cobalt shows lower ASR values compared to a bare sample. These lower values are due to the formation of Co_3O_4. After 1000 h the ASR value for the sample without cobalt was 1.30 Ω cm^{-2} and for sample with a cobalt film it was 0.038 Ω cm^{-2}.

Acknowledgments The authors acknowledge UFMG, CNPq and CEMIG for financial support. A special acknowledgement to Michel Kleitz by revision.

References

1. Singhal SC, Kendall K (2004) High temperature solid oxide fuel cells: fundamentals designs and applications, 2nd edn. Elsevier Science, Oxford, pp 103–110
2. Lang M, Franco T, Schiller G, Wagner N (2002) J Appl Electrochem 32:871
3. Piccardo P, Amendola R, Fontana S et al (2009) J Appl Electrochem 39:534
4. Fergus JW (2005) J Power Sources 397:271
5. Chevalier S, Caboche G, Przybylski K et al (2009) J Appl Electrochem 39:529
6. Repetto L, Costamagna P (2008) J Appl Electrochem 38:1005
7. Shaigana N, Qua W, Ivey DG et al (2010) J Power Sources 195:1529
8. Liu Y, Chen DY (2009) Int J Hydrogen Energy 34:9220
9. Petric A, Ling H (2007) J Am Ceram Soc 5:1515
10. Stanislowski M, Froitzheim J, Niewolak L et al (2007) J Power Sources 164:578
11. Deng X, Wei P, Bateni MR et al (2006) J Power Sources 160:1225
12. Wu J, Jiang Y, Johnson C, Liu X (2008) J Power Sources 177:376
13. Lupi C, Pasquali M, Era AD (2005) Waste Manage 25:215
14. Freitas MBJG, Garcia EM, Celante VG (2009) J Appl Electrochem 39:601
15. Freitas MBJG, Garcia EM (2007) J Power Sources 171:953
16. Santos JS, Matos R, Strixino FT et al (2007) Electrochim Acta 53:122
17. Matsushima T, Strixino FT, Pereira EC (2006) Electrochim Acta 51:1960
18. Garcia EM, Santos JS, Pereira EC et al (2008) J Power Sources 185:549
19. Hansson AN, Linderoth S, Mogensen M et al (2007) J Alloys Compd 433:193